# Highly Efficient Solar Steam Generation by $W_{18}O_{49}$@PVA Gels

Jiefeng Yan †, Zhenxing Fang †, Jinxing Hu, Yangming Sun, Xinyi Huang, Guannan Zhou, Lu Li *, Rui Wang, Yan Chen

Posted Date: 2 September 2025

doi: 10.20944/preprints202509.0108.v1

Keywords: oxygen-deficiency; tungsten oxide; NIR adsorption; solar steam generation; cross-linking gel

*Article*

# Highly Efficient Solar Steam Generation by $W_{18}O_{49}$@PVA Gels

**Jiefeng Yan [1,†], Zhenxing Fang [1,†], Jinxing Hu [1], Yangming Sun [1], Xinyi Huang [1], Guannan Zhou [2], Lu Li [2,*], Rui Wang [2] and Yan Chen [3]**

[1] College of Science and Technology, Ningbo University, Ningbo Key Laboratory of Agricultural Germplasm Resources Mining and Environmental Regulation, Ningbo, Zhejiang, 315300, China

[2] Division of Energy Materials (DNL2200), Dalian Institute of Chemical Physics, Chinese Academy of Sciences, Dalian, 116023, P. R. China

[3] State Key Laboratory of Inorganic Synthesis and Preparative Chemistry, Jilin University, Changchun 130012, China

* Correspondence: author: lilu528@dicp.ac.cn

† These authors contributed equally to this work.

**Abstract**

The oxygen deficient tungsten oxide $W_{18}O_{49}$ was synthesized through lattice oxygen escaping at high temperature in $N_2$ atmosphere. The temperature and inert atmosphere were critical conditions to initiate the lattice oxygen escaping to obtain $W_{18}O_{49}$. The synthesized tungsten oxides were characterized by X-ray diffraction (XRD), scanning electron microscopy (SEM), X-ray photoelectron spectroscopy (XPS), ultraviolet photoelectron spectroscopy (UPS) and ultraviolet-visible absorption spectroscope (UV-Vis). The composite gel was fabricated by the oxygen deficient tungsten oxide insertion into PVA-based gel, which was cross linked by glutaraldehyde. The gel was characterized by Fourier transform infrared (FTIR) spectroscopy and solar steam generation test. The result of the solar steam generation shows that the $W_{18}O_{49}$-PVA gel (steam generation rate 2.63 kg $m^{-2}$ $h^{-1}$) was faster than that of the pure PVA gel.

**Keywords:** oxygen-deficiency; tungsten oxide; NIR adsorption; solar steam generation; cross-linking gel

## 1. Introduction

The shortage of freshwater resources and the pressure of energy consumption are increasingly becoming global challenges. Traditional seawater desalination and wastewater treatment technologies often come with high energy consumption and high cost issues. In recent years, Interfacial Solar Steam Generation (ISSG) technology, characterized by its utilization of green solar energy, low system heat capacity, and high evaporation efficiency, has emerged as a promising sustainable solution [1,2]. The core of this technology lies in the development of efficient photothermal conversion materials and the optimization of evaporator structure design for water/heat management.

ISSG technology achieves efficient capture and conversion of solar energy by localizing photothermal materials at the gas-liquid interface, and maximally confines heat near the evaporation interface, significantly reducing heat loss to the bulk of the water body. The ideal performance relies on three core points: broad-spectrum efficient light absorption, excellent photothermal conversion, and intelligent water/heat management. However, traditional photothermal materials (such as carbon-based materials, noble metal nanoparticles, and semiconductors) may suffer from issues such as narrow light absorption bands, high cost, and insufficient stability [3–5]. It is urgent to develop novel, efficient, low-cost, easily integratable material systems that can synergistically optimize light-heat-water transport [6].

 doi:10.20944/preprints202509.0108.v1



The commercial $WO_3$ has a band gap of 2.5-2.8 eV which absorbs little visible light. Doping some hetero-valence metal ions or introducing some oxygen vacancies are the common methods to improve the concentration of free-carries so as to enhance the light absorption. Tungsten oxide could withstand a large amount of oxygen vacancies so as to the formation of various phases. Non-stoichiometric tungsten oxides ($WO_{3-x}$) have attracted increasing interest due to their unique properties [7]. Among these, $W_{18}O_{49}$ is a particularly important member of the $WO_{3-x}$ family, which contains the largest amount of oxygen deficiency. Extensively, its preferential growth and exceptional chemical stability makes it excellent performance in various fields [8–10]. Notably, $W_{18}O_{49}$ nanowires are particularly versatile, retaining all the characteristic properties of bulk $W_{18}O_{49}$ while also exhibiting a high aspect ratio. This morphology facilitates the efficient transfer of photo-generated carriers along the nanowire axis which is important for achieving efficient photothermal conversion. Up to now, various methods have been successfully developed to synthesize $W_{18}O_{49}$ tungsten oxide, including solvothermal [11], thermal evaporation [12], hydrothermal [13,14], simple reflux [15], microwave-assisted [16] and electron beam irradiation [17] and so on. In this report, the oxygen deficient tungsten oxide $W_{18}O_{49}$ was synthesized through lattice oxygen escaping at high temperature in $N_2$ atmosphere.

In order to boost the water evaporation efficiency, a fast water supply to the evaporation surface is especially important. Therefore, a hydrophilic network such as PVA should be introduced into the structure of evaporator. PVA hydrogel could play a crucial dual role as a “water channel” and “thermal barrier” in ISSG evaporators due to its unique three-dimensional network structure [18–22]. Firstly, the PVA network rich in hydroxyl (-OH) groups exhibits strong hydrophilic nature, enabling rapid absorption of water from the underlying layer through capillary forces. Its porous structure provides continuous and low-resistance transmission channels for water molecules, ensuring continuous and sufficient water supply to the evaporation interface and preventing local drying. Secondly, the PVA polymer backbone itself is a poor conductor of heat. The heat generated inside the gel can be used to provide the latent heat (~2260 kJ/kg) required by internal water molecules during evaporation, effectively limiting the diffusion of heat to the bulk of the water body and efficiently “locking” the thermal energy at the evaporation interface, significantly improving heat utilization efficiency [23]. Furthermore, PVA hydrogel possesses excellent flexibility, biocompatibility, and processability (such as freeze-thaw cycling and chemical crosslinking), facilitating the integration of different nanomaterials and enabling the construction of diversified and adaptable (such as flexible and wearable) evaporator structures. Therefore, ingenious material design and structural optimization of $W_{18}O_{49}$/PVA composite gel can effectively synergize light harvesting, heat generation, water supply, and thermal management, providing a practical approach to achieve ultra-high evaporation efficiency.

## 2. Results and Discussion

Figure 1 shows the XRD patterns of tungsten oxide obtained from various temperature in air or $N_2$ atmosphere. It was obvious to distinguish that only the XRD pattern of tungsten oxide obtained at 900 °C under $N_2$ atmosphere was different from that of other three tungsten oxide samples. At the lower annealing temperature 700 °C, the XRD patterns of products shows monoclinic $WO_3$ no matter with the air or $N_2$ condition, which matches well with the JCPDS No.43-1035. The XRD pattern of tungsten oxide obtained at 900 °C under air condition shows a sharper diffraction peaks than that of samples obtained at 700 °C. This is due to the improved crystallinity of the tungsten oxide at higher temperature. Whereas XRD pattern of tungsten oxide obtained at 900 °C under $N_2$ condition shows monolinic $W_{18}O_{49}$ matches well with the JCPDS No.71-2450. This large amount of oxygen vacancy is caused by lattice oxygen escaping and $WO_6$ octahedron unit cell rearrangement under inert atmosphere at high temperature. The appearance of the product shows a dark blue which is also widely different with that of other three samples.

 doi:10.20944/preprints202509.0108.v1



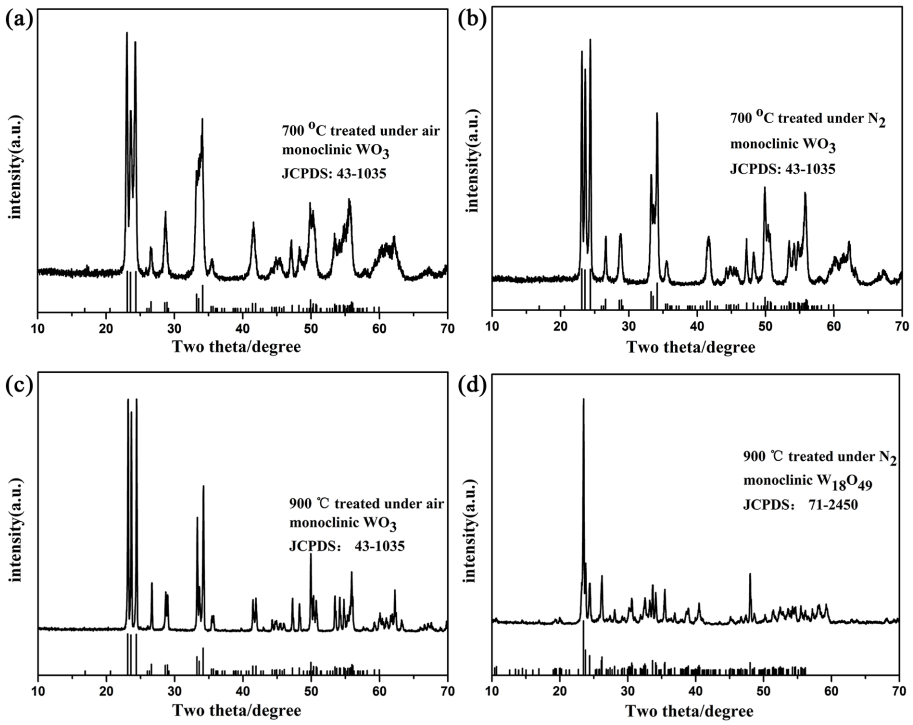


**Figure 1.** XRD patterns of obtained products at different temperatures.

Figure 2 shows the SEM images of these tungsten oxides obtained in various conditions. The morphology of tungsten oxide obtained at 700 °C was basically consistent in air or $N_2$, which shows nanoplate morphology with a 200 nm radius and 50 nm thickness. When the annealing temperature reached up to 900 °C, the morphology of tungsten oxide turns to be larger particles whose size is larger than 1 um. This is also evidenced by the result of its XRD shown in Figure 1c. The sharper XRD peaks also reveal a larger particle size. It's interesting that the morphology turns out to be nanorods when the annealing treatment was 900 °C in $N_2$. This is also consistent with other reported $W_{18}O_{49}$ material which has preferential growth in *b* axis direction. It should be noted that $N_2$ surrounding differs the reduced atmosphere as $H_2$ or $H_2/N_2$ mixed atmosphere. In a strong reduced atmosphere, a large amount of lattice oxygen in $WO_3$ would be eliminated so as to form many other phases such as $WO_{2.9}$, $WO_{2.83}$ or mixed phases and so on [24]. However, in an inert atmosphere, the result shows that the lattice oxygen in $WO_3$ is stable even at 700 °C and lattice oxygen escape occurred at 900 °C so as to the formation of $W_{18}O_{49}$. Thus, we proposed a new method to synthesize $W_{18}O_{49}$ at 900 °C in $N_2$.

 doi:10.20944/preprints202509.0108.v1



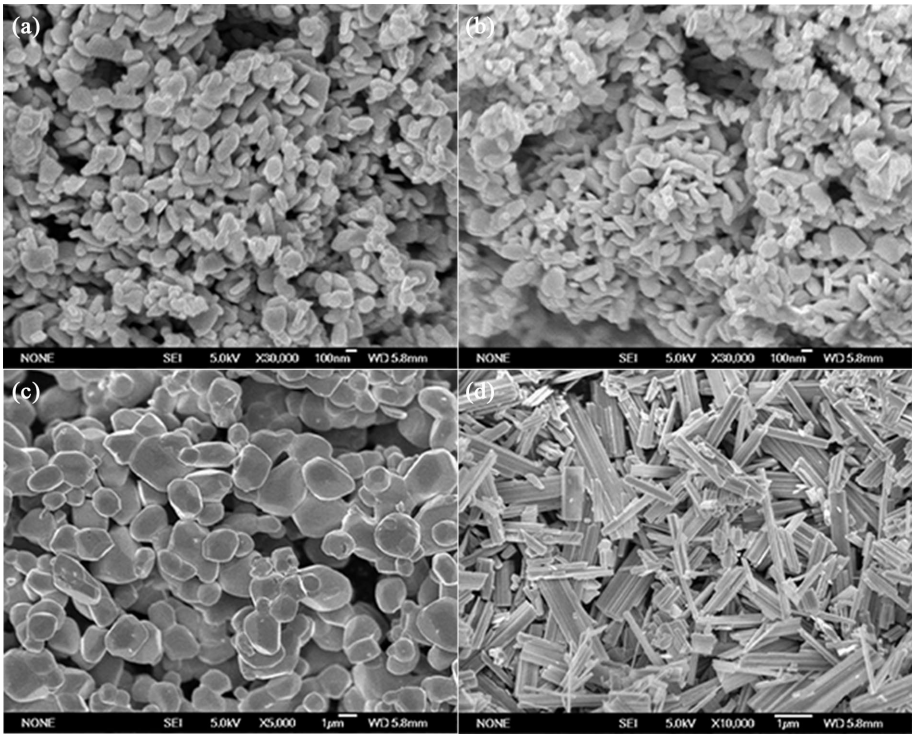


**Figure 2.** SEM images of tungsten oxide. (**a**)700 °C air, (**b**) 700 °C $N_2$, (**c**) 900 °C air, and (**d**) 700 °C $N_2$.

As the lattice oxygen in tungsten oxide escaped at high temperature in $N_2$, large amounts of oxygen defect generated which drive the $WO_6$ octahedron unit cell rearrangement to form a more stable phase $W_{18}O_{49}$. Thus, XPS was conducted to survey the oxidation state of W in the new generated product. Figure 3 shows the XPS spectrum of W 4f orbital in the dark blue sample. The broad shoulder peak in Figure 3 reveals a mixed oxidation state of W. The doublet peaks at about 37.8 and 35.7 eV are assigned to W $4f_{5/2}$ and W $4f_{7/2}$ of $W^{6+}$, respectively. The lower binding energy peaks at 36.4 and 34.3 eV belong to W $4f_{5/2}$ and W $4f_{7/2}$ of $W^{5+}$, respectively [25]. The percentage of $W^{5+}$ is calculated to be 32.5% according to the integral areas of the peaks. The XPS spectra of other three tungsten oxide samples do not have a shoulder peak. Its high symmetrical peak reveals the absence of reduced tungsten state ($W^{5+}$). Thus, the temperature and atmosphere are both critical for the synthesis of $W_{18}O_{49}$.

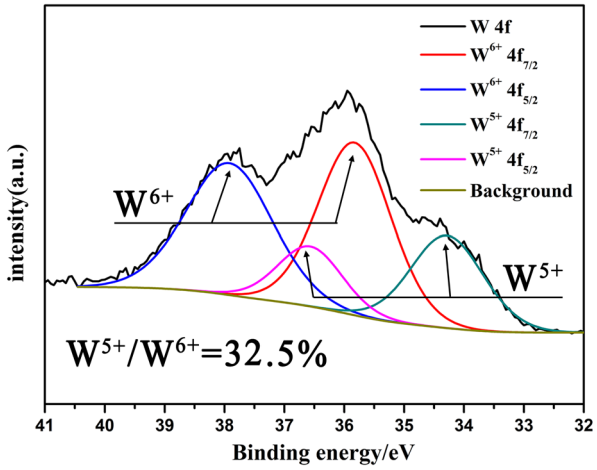


**Figure 3. W 4f orbital** XPS spectrum of tungsten oxide obtain at 900 °C in $N_2$.

 doi:10.20944/preprints202509.0108.v1



The appearance of these tungsten oxides obtained in various conditions was extremely different. The reduced tungsten oxidation state ($W^{5+}$) is often regarded as the color center in tungsten oxide. Therefore, the oxygen deficient product exhibits a dark blue appearance which differs from that of other tungsten oxides. As shown in Figure 4a, the green line shows a broad adsorption during the whole UV-Vis range while the products obtained at 700 °C only shows a slight adsorption during the visible light range. The red line also exhibits partial adsorption in visible range due to its increased crystallinity. The partial red light adsorption results in a green appearance of this tungsten oxide powder. The band gap of these tungsten oxides was calculated according to the absorbance. As shown in Figure 4b, the black line and red line represents the sample obtain at 700 °C, demonstrated to be a similar band gap about 2.5 eV [26,27]. The blue line shows a smaller band gap due to its higher crystallinity. A more orderly arrangement of $WO_6$ units causes more absorbance. However, the strong absorbance during the whole UV-Vis range of $W_{18}O_{49}$ reveals its "*quasi*-conductor" property which comes from its high concentration of free carries. These results are similar to the previous reported research, the light adsorption capability increases with the increment of free carriers in transition metal oxide semiconductor [28]. A self-floating evaporator with a stable photothermal conversion performance of $W_{18}O_{49}$ coupled with carbon foam has been reported and applied in solar steam generation [29]. Here, a fine designed hydrophilic gel was adopted to play a crucial dual role as a "water channel" and "thermal barrier" so as to significantly increase the evaporation efficiency.

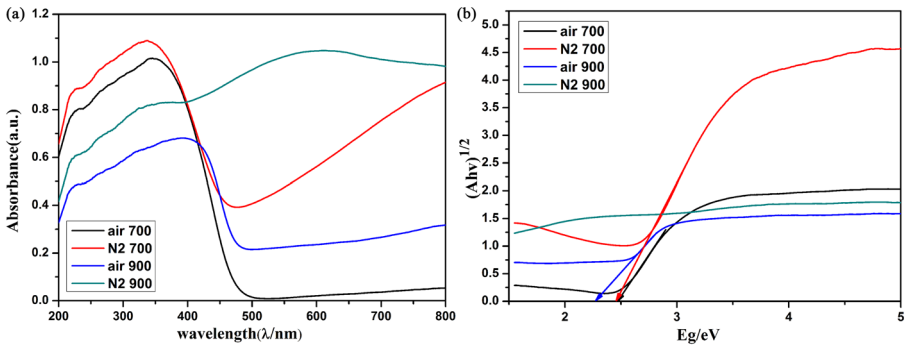


**Figure 4.** (a) Adsorption spectra of the tungsten oxide obtained in various conditions, (b) calculated band gap of these tungsten oxides.

Figure 5 shows the FTIR spectrum of the composite gel. The PVA chains are rich in hydroxyl groups, which could be cross-linked by glutaraldehyde in acid condition results in the formation of three-dimensional interpenetrating network structure. The molecular with a head-to-tail dialdehyde structure is often used to crosslink the long chain polymer with hydroxyl groups [30–32]. This interconnected PVA structure could serve as thermal barrier in ISSG evaporators due to its low thermal conductivity. Moreover, it also reserves partial hydroxyl groups (as shown the strong adsorption at ~3500 $cm^{-1}$). This reservation of hydroxyl groups ensures its hydrophilicity which is critical to the water transportation in ISSG technology. Therefore, the composite gel plays a crucial dual role as a "water channel" and "thermal barrier" in ISSG evaporators due to its unique three-dimensional network structure.

 doi:10.20944/preprints202509.0108.v1



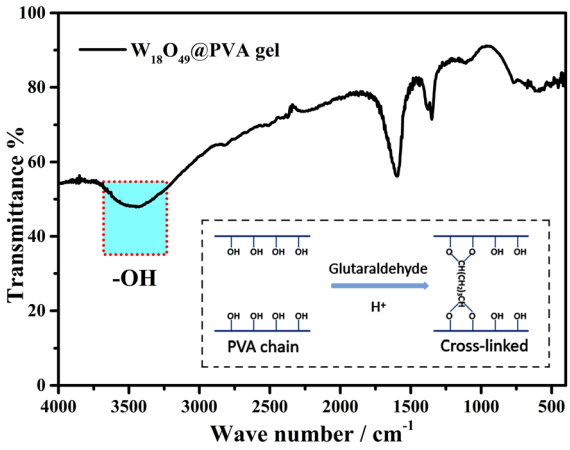


**Figure 5.** FTIR spectra of the $W_{18}O_{49}$@PVA gels.

The solar steam generation test was conducted under 1 sun irradiation to estimate the practical performance of this well-designed composite gel. The mass change represents the amount of evaporated water, which was recorded by 1 min interval. It is obvious to see that the vapor generation with composite gel is more efficient than that of pure water or pure PVA gel. All the experimental data of solar vapor generation are calibrated to dark-condition evaporation data. The black line represents the evaporation rate of pure water, which was calculated to be 0.39 kg/m$^2$. The evaporation rate of the cross linked PVA gel was 0.53 kg/m$^2$ which is faster than that of pure water. The heat loss decreases due to its polymer nature of low thermal conductivity. Whereas the surface heat generation was limited due to the lack of effective photothermal conversion material. When the PVA gel coupled with oxygen deficient rich material $W_{18}O_{49}$, the vapor generation rate was remarkably improved. Furthermore, the evaporation rate also accelerates as the amount of $W_{18}O_{49}$ increases. The max evaporation rate of 5wt% $W_{18}O_{49}$@PVA gel reaches up to 2.65 kg/m$^2$, which is more than 6 times to the pure water. The temperature of this evaporation surface is less than 40 °C due to the fast water evaporation. This also reveals that the localized heat generation was almost used in the phase change of water and there is no much heat loss. It could be concluded that a suitable water supply couples the localized heat generation results in a high solar utilization and water evaporation rate. This fast evaporation rate was benefit from the reduced vaporization enthalpy, which comes from the water cluster theory. This theory reveals that water can be evaporated as either a single molecule or in small clusters consisting of a few to tens of molecules. Thus, this hydrophilic PVA gel plays two key roles as a “water channel” and “thermal barrier”, which resulting a reduced vaporization enthalpy so as to improve the water evaporation rate.

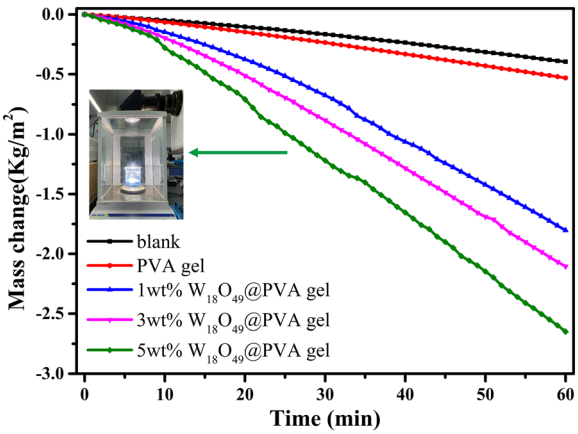

 doi:10.20944/preprints202509.0108.v1



**Figure 6.** Solar steam generation test under 1 sun irradiation (inserted image was the $W_{18}O_{49}$@ PVA gel irradiated by simulated solar light).

## 3. Conclusions

A highly efficient interfacial solar steam generation system was well designed by insertion $W_{18}O_{49}$ into PVA base gel. The photothermal conversion material of $W_{18}O_{49}$ was successfully synthesized through direct annealing at 900 °C in $N_2$. The PVA gel still keeps hydrophilic nature after cross linked by glutaraldehyde which is essential for its water transportation. The composite $W_{18}O_{49}$@PVA gel exhibits a fast water evaporation rate 2.65 kg/m$^2$ which is more than 6 times of pure water. This enhancement is attributed to the coupling efficient light absorption and heat conversion properties of $W_{18}O_{49}$ nanorods and the water transportation of PVA gel, which significantly improve the overall performance of the composite gel. This type of solar steam evaporator might be used for many other applications, including environmental cooling, seawater desalination, and pollution abatement.

## 4. Materials and Methods

### *4.1. Materials*

Tungsten(VI) oxide, $WO_3$ (purity lager than 99.8%) was purchased from Aladdin (Shanghai, China). Poly(vinyl alcohol)(PVA) $M_w$=31000-50000 and Glutaraldehyde 50% in water (Analytical Reagent) were also purchased from Aladdin (Shanghai, China). There was no need to purify before use. HCl was diluted to 1M to catalysis the cross linking reaction. High purity $N_2$ (99.999%) was purchase from Cixi Qunying Gas Co., Ltd. Deionized water (conductivity less than 10 μS/cm) was self-made to wash the gel.

### *4.2. Procedures of the Composite Gel Synthesis*

#### 4.2.1. The Synthesis of Tungsten Oxide

Position the commercial yellow tungsten trioxide powder at the center of the tubular furnace. Initially, purge high-purity (99.999%) nitrogen into the tube for 30 minutes to extrude the air. Subsequently, heat the powder to the setting temperature at a ramping rate of 10°C/min and keep for 2 hours. Allowing it to cool down to room temperature, oxygen deficient tungsten oxide product was obtained. For the purpose of comparing the impact of different atmospheres on the products, tungsten oxide materials were also prepared under identical heat treatment conditions in air for comparative analysis. The prepared series products were labeled as $N_2$-700, $N_2$-900 and Air-700, Air-900 for different tungsten oxide, respectively. The Air-700 and Air-900 tungsten oxide are yellow powders and the $N_2$-700, $N_2$-900 shows a pine green and dark blue appearance, respectively.

#### 4.2.2. Preparation of PVA Gel

PVA (1 g), glutaraldehyde (125 μL, 50%wt in DI water) and Dl water (10 mL) were mixed together by sonication (solution C). Then HCl (50 μL, 1.0M) were added to 10 mL of solution C, the gelation was carried out for 12 h, the obtained cross-linked gel was immersed into DI water overnight to remove the impurity. The purified composite gel was frozen by liquid nitrogen and then thawed in DI water at a temperature of 30 °C, The freezing-thawing process was repeated for 5 times. Finally, the obtained HNG sample was freeze-dried.

#### 4.2.3. Preparation of $W_{18}O_{49}$@PVA Composite Gel

In a typical synthesis, PVA (1 g), glutaraldehyde (125 μL, 50%wt in DI water) and Dl water (10 mL) were mixed together by sonication (solution C). Then HCl (50 μL, 1.0M) and a certain amount of $W_{18}O_{49}$ (1wt%, 3wt% and 5wt% according to the mass of PVA) were added to 10 mL of solution C, the gelation was carried out for 12 h, the obtained composite gel was immersed into DI water

 doi:10.20944/preprints202509.0108.v1



overnight to remove the impurity. The purified composite gel was frozen by liquid nitrogen and then thawed in DI water at a temperature of 30 °C, The freezing-thawing process was repeated for 5 times. Finally, the obtained HNG sample was freeze-dried.

#### 4.2.4. Experiment of Solar Steam Generation

The solar steam generation test was conduct at 25 °C irradiated by simulated solar light(AM1.5 without condensing lens, irradiation power 1 kW/m$^2$). The distance from the gel surface to the simulated light keeps 20 cm. The outer space of the container was totally contact with the surrounding, which is without the covering of thermal insulation foam. The mass change was recorded by 1 min interval during the solar irradiation. The mass change of the system without irradiation was also recorded by 1 min interval to represent the dark-condition water evaporation. And thermal camera was used to record the gel surface temperature, which directly demonstrates the water evaporation effect.

### *4.3. Characterization*

The XRD patterns were recorded by using PANalytical B.V. Empyrean X-ray powder diffraction (Malvern Panalytical, Enigma Business Park, Grovewood Road, Malvern, WR14 1XZ, United Kingdom) with Cu K$\alpha$ radiation over a range of 10–70° (2$\theta$) with 0.02° per step, scanning rate 10°/min. SEM images were obtained with a JSM-6700F electron microscope (JEOL, 1-2 Musashino 3-chome, Showa City, Tokyo), operating voltage 5 kV, working current 10 mA. X-ray photoelectron spectrometer was recorded by ESCALAB 250 (Thermal Fisher, America). UV-Vis spectra was recorded by Lambda 950 (PerkinElmer, America). The FTIR spectrum was recorded by Fourier Transform Infrared Spectrometry FTIR-650. The mass change was recorded by electronic analytical balance (FA2004).

**Author Contributions:** Conceptualization, Jiefeng Yan, and Zhenxing Fang; methodology, Yangming Sun and Xinyi Huang; software, Jinxing Hu and Guannan Zhou; validation, Lu Li and Rui Wang; formal analysis, Zhenxing Fang; investigation, Jinxing Hu; resources, Yan Chen and Jinxing Hu; writing—original draft preparation, Jiefeng Yan; writing—review and editing, Zhenxing Fang and Jinxing Hu.; supervision, Jiefeng Yan; project administration, Jinxing Hu and Rui Wang; funding acquisition, Rui Wang. All authors have read and agreed to the published version of the manuscript.

**Funding:** This research was funded by National Key Research and Development Program of China (2022YFC2105800).

**Institutional Review Board Statement:** This did not require ethical approval.

**Informed Consent Statement:** The study did not involve humans.

**Data Availability Statement:** The data presented in this study are openly available in article.

**Acknowledgments:** Thanks to the General scientific research projects of Zhejiang Provincial Department of Education (Y202352630) and the Open project of the State Key Laboratory of Inorganic Synthesis and Preparative Chemistry, Jilin University (2023-22).

**Conflicts of Interest:** The authors declare no conflicts of interest.

## References

1. Abdullah, H., et al., A Brief Review of Emerging Strategies in Designing Interfacial Solar Steam Generation for Desalination, Water Purification, Power Generation, and Sea Farming. *ACS Applied Energy Materials*, **2025**. *8*(5):2663-2704.
2. Zhang, Z., et al., Bio-based interfacial solar steam generator. *Renewable and Sustainable Energy Reviews*, **2024**. *203*:114787.

 doi:10.20944/preprints202509.0108.v1




3. Ibrahim, I., et al., Semiconductor photothermal materials enabling efficient solar steam generation toward desalination and wastewater treatment. *Desalination*, **2021**. *500*:114853.
4. Yong Wang, et al., Plasmonic Photothermal Nanomaterials for Solar Steam Generation. *Chem. Sci.*, **2025**:Accepted Manuscript.
5. Zhu, J., et al., Carbon materials for enhanced photothermal conversion: Preparation and applications on steam generation. *Materials Reports: Energy*, **2024**. *4*(2):100245.
6. Hou, J., et al., Review on the structural design of solar-driven interfacial evaporation. *Journal of Environmental Chemical Engineering*, **2025**. *13*(3):116462.
7. Tang, Y., et al., Functional Aerogels Composed of Regenerated Cellulose and Tungsten Oxide for UV Detection and Seawater Desalination. *Gels*, **2022**. *9*(1).
8. Sun, X., et al., Controlled assembly and synthesis of oxygen-deficient $W_{18}O_{49}$ films based on solvent molecular strategy for electrochromic energy storage smart windows. *Chemical Engineering Journal*, **2024**. *499*:156109.
9. Xiong, Y., et al., Facile synthesis of hierarchical $W_{18}O_{49}$ microspheres by solvothermal method and their optical absorption properties. *Discov Nano*, **2024**. *19*(1):89.
10. Yan, N.-F., et al., Recent progress of $W_{18}O_{49}$ nanowires for energy conversion and storage. *Tungsten*, **2023**. *5*(4):371-390.
11. Qiu, Y. and Y. Wang, Controllable synthesis of $W_{18}O_{49}$ nanoneedles for high-performance $NO_2$ gas sensors. *Journal of Alloys and Compounds*, **2023**. *944*:169199.
12. Li, Y., Y. Bando, and D. Golberg, Quasi-Aligned Single-Crystalline $W_{18}O_{49}$ Nanotubes and Nanowires. *Advanced Materials*, **2003**. *15*(15):1294-1296.
13. Chen, H., et al., PABA-assisted hydrothermal fabrication of $W_{18}O_{49}$ nanowire networks and its transition to $WO_3$ for photocatalytic degradation of methylene blue. *Advanced Powder Technology*, **2018**. *29*(5):1272-1279.
14. Gao, X., et al., Hydrothermal fabrication of $W_{18}O_{49}$ nanowire networks with superior performance for water treatment. *Journal of Materials Chemistry A*, **2013**. *1*(19):5831.
15. Zhou, G., et al., Oxygen-Sensitive Nanomaterials Synthesized in an Open System: Water-Triggered Nucleation and Its Controllability in the Growth Process. *Inorg Chem*, **2025**. *64*(14):6811-6815.
16. Nayak, A.K. and D. Pradhan, Microwave-Assisted Greener Synthesis of Defect-Rich Tungsten Oxide Nanowires with Enhanced Photocatalytic and Photoelectrochemical Performance. *The Journal of Physical Chemistry C*, **2018**. *122*(6):3183-3193.
17. Guozhen Shen, et al., Electron-Beam-Induced Synthesis and Characterization of $W_{18}O_{49}$ Nanowires. *J. Phys. Chem. C*, **2008**. *112*(112):5856-5859.
18. Li, J., et al., Porous polyvinyl alcohol/biochar hydrogel induced high yield solar steam generation and sustainable desalination. *Journal of Environmental Chemical Engineering*, **2022**. *10*(3):107690.
19. Li, N., et al., Bioinspired Flexible Composite Hydrogels for Efficient Solar Steam Generation and Stable Electricity Harvest. *Nano Lett*, **2025**. *25*(25):10072-10081.
20. Shi, Y., et al., All-day fresh water harvesting by microstructured hydrogel membranes. *Nat Commun*, **2021**. *12*(1):2797.
21. Tian, Y., et al., Versatile PVA/CS/CuO aerogel with superior hydrophilic and mechanical properties towards efficient solar steam generation. *Nano Select*, **2021**. *2*(12):2380-2389.
22. Xu, X., et al., Full-spectrum-responsive $Ti_4O_7$-PVA nanocomposite hydrogel with ultrahigh evaporation rate for efficient solar steam generation. *Desalination*, **2024**. *577*:117400.
23. Zhao, F., et al., Highly efficient solar vapour generation via hierarchically nanostructured gels. *Nat Nanotechnol*, **2018**. *13*(6):489-495.
24. Zhang, J., et al., $W_{18}O_{49}$ nanorods: Controlled preparation, structural refinement, and electric conductivity. *Chemical Physics Letters*, **2018**. *706*:243-246.
25. Fang, Z., et al., Photothermal Conversion of $W_{18}O_{49}$ with a Tunable Oxidation State. *ChemistryOpen*, **2017**. *6*(2):261-265.
26. Parikh, D., H. Yadav, and S. Kapatel, Machine learning-based prediction of optical band gap in $WO_3$ and its derivatives for semiconducting applications. *Optik*, **2023**. *291*:171310.

 doi:10.20944/preprints202509.0108.v1




27. Vemuri, R.S., M.H. Engelhard, and C.V. Ramana, Correlation between surface chemistry, density, and band gap in nanocrystalline $WO_3$ thin films. *ACS Appl Mater Interfaces*, **2012**. *4*(3):1371-7.
28. He, M., et al., Remarkable enhancement of the nonlinear optical absorption of $W_{18}O_{49}$ by Cu doping. *Materials Today Physics*, **2024**. *42*:101357.
29. Fang, Z., et al., A Flexible, Self-Floating Composite for Efficient Water Evaporation. *Glob Chall*, **2019**. *3*(6):1800085.
30. Gao, M.-h., et al., Glutaraldehyde-assisted crosslinking in regenerated cellulose films toward high dielectric and mechanical properties. *Cellulose*, **2022**. *29*(15):8177-8194.
31. Jeon, J.G., et al., Cross-linking of cellulose nanofiber films with glutaraldehyde for improved mechanical properties. *Materials Letters*, **2019**. *250*:99-102.
32. Zhang, F., et al., Glutaraldehyde-assisted crosslinking for the preparation of low dielectric loss and high energy density cellulose composites filled with poly(dopamine) modified MXene. *European Polymer Journal*, **2024**. *221*:113526.